



Noise-induced escape of a self-propelled particle from metastable orbitsRubens H. Damascena  and Clécio C. de Souza Silva **Departamento de Física, Centro de Ciências Exatas e da Natureza, Universidade Federal de Pernambuco, Recife-PE, 50670-901, Brasil*

(Received 26 August 2023; accepted 6 October 2023; published 31 October 2023)

Active particles, like motile microorganisms and active colloids, are often found in confined environments where they can be arrested in a persistent orbital motion. Here, we investigate noise-induced switching between different coexisting orbits of a confined active particle as a stochastic escape problem. We show that, in the low-noise regime, this problem can be formulated as a least-action principle, which amounts to finding the most probable escape path from an orbit to the basin of attraction of another coexisting orbit. The corresponding action integral coincides with the activation energy, a quantity readily accessible in experiments and simulations via escape rate data. To illustrate how this approach can be used to tackle specific problems, we calculate optimum escape paths and activation energies for noise-induced transitions between clockwise and counterclockwise circular orbits of an active particle in radially symmetric confinement. We also investigated transitions between orbits of different topologies (ovals and lemniscates) coexisting in elliptic confinement. In all worked examples, the calculated optimum paths and minimum actions are in excellent agreement with mean-escape-time data obtained from direct numerical integration of the Langevin equations.

DOI: [10.1103/PhysRevE.108.044605](https://doi.org/10.1103/PhysRevE.108.044605)**I. INTRODUCTION**

The problem of noise-induced escape from a meta-stable state is a fundamental challenge in physics, chemistry, and biology, with implications for fields such as materials science, biophysics, and neuroscience. In many cases, this problem can be modeled as the escape of a Brownian particle from a local minimum of a potential energy landscape through a saddle point, with the mean escape time following the classical Kramers formula [1,2]. However, this model has limitations in describing noise-induced escape problems in systems where the activation energy depends not only on the endpoints but also on the specific shape of the escape trajectory, that is, systems that cannot be reduced to an effective potential energy. These systems include driven Josephson junctions [3,4], particles in parametrically excited traps [5,6], and excitable neuronal models [7,8], among others. The complexity of these problems adds considerable challenge to the task of understanding and predicting noise-induced escape dynamics.

The escape of active Brownian particles from local minima is a particularly interesting example of an activation problem that depends on the specific escape path [9–18]. This problem has received a lot of attention recently, in part because of the increasing interest in predicting and controlling the behavior of small self-propelled entities in various applications, from drug delivery and nanorobotics to bacterial motility and collective behavior. These particles are endowed with persistent motion [19–21], typically modeled as a self-propulsion force of constant intensity, which allows them to climb an external potential landscape up to a point where their propulsion force

is canceled out by the confining force [22–27]. At this point, the particle stalls but thermal noise can assist it to climb further away and eventually escape the potential well. Woillez *et al.* [13] have shown that the low-noise escape time for this problem still follows Kramers exponential form, but with the potential barrier replaced by a pseudo-potential that depends on both the confining potential and the particle’s propulsion speed, leading to a range of interesting phenomena. For instance, the particle may “choose” to escape through a lower or higher barrier height, depending on the propulsion speed.

Some self-propelled microorganisms, like motile *Chlamydomonas* algae [28] and *Magnetospirillum* bacteria [29], prefer to orbit around the center of a confining potential rather than climbing it up to the stall point. A similar orbital motion is reproduced by a hexbug robot in a parabolic reflector [30]. Common to these systems is that their dynamics can be successfully modeled by adding an aligning torque to the equation of motion of the particle’s orientation vector. This torque couples the orientation vector to the local force field and induces spontaneous symmetry breaking, creating the possibility of either clockwise or counterclockwise circular orbits [30]. When the potential lacks radial symmetry, as in the case of elliptic confinement, the particle can perform a variety of complex orbits, with distinct, well-defined topological indices [31]. Interestingly, two or more of these orbits can coexist in the same region of the parameter space. These observations pose a noise-induced escape problem fundamentally different from the ones previously discussed: the decay of a confined active particle from a metastable orbit into another without ever leaving the confining potential. Indeed, noise-induced transitions between such orbits have been reported [29–31], but an in-depth study on how the escape rate depends on the noise intensity and insights on the escape dynamics are still lacking.

*clecio.cssilva@ufpe.br

In the present work, we tackle this problem in the framework of a least-action principle. We show that the low-noise transition probability is dominated by the path that minimizes the classical action, resulting in a Kramers-like exponential escape time, $t_{\text{esc}} \sim \exp(S/D)$, where S is the action integral along the most probable escape path (MPEP). This path is found by solving the deterministic equations of motion of an auxiliary Hamiltonian, derived from the least-action principle. The details of this approach are presented in Sec. II. Then, we apply this formalism to analyze two distinct scenarios, presented respectively in Secs. III and IV. In the first one, we investigate transitions between clockwise and counterclockwise circular orbits of an active particle in radially symmetric confinement. In the limit of strong (hard-wall) confinement, we show that this problem is reduced to the original Kramers escape problem, with the effective potential being a function of the orbit radius and the propulsion speed of the particle, and derive an analytical expression for the escape rate. For moderate or weak confinement, the problem can no longer be defined in terms of an effective potential. In this case, we find the optimum escape path numerically by minimizing the action integral between the orbit and the boundary of its basin of attraction. In the second scenario, we calculate the optimum escape paths and corresponding escape rates for noise-induced transitions between multiple orbits of different topological indexes for the case of elliptic confinement. In all cases, the minimum action approach is shown to be in excellent agreement with direct numerical simulations of the Langevin equations of motion of the active particle. Conclusions and outlook of the work are given in Sec. V.

II. GENERAL FORMULATION

A. Model system and competing orbits

We consider an overdamped active particle in the (x, y) plane subjected to a confining, conservative force field $\mathbf{F}(\mathbf{r})$ and a generic off-plane torque $\hat{z}\tau$. The corresponding translational and rotational dynamics are modeled by the following Langevin equations:

$$\dot{\mathbf{r}} = v_0 \hat{\mathbf{n}} + \mu \mathbf{F} + \boldsymbol{\zeta}(t), \quad (1)$$

$$\dot{\theta} = \beta \tau + \xi(t), \quad (2)$$

where $\hat{\mathbf{n}} = (\cos \theta, \sin \theta)$ is the particle orientation axis, v_0 is the self-propulsion speed, and μ (β) is the translational (angular) mobility. The stochastic forces $\xi(t)$ and $\zeta(T)$ are independent Gaussian noises of zero mean and correlation

$$\langle \zeta_\mu(t) \zeta_\nu(t') \rangle = 2D_t \delta_{\mu\nu} \delta(t - t'), \quad (3)$$

$$\langle \xi(t) \xi(t') \rangle = 2D_r \delta(t - t'), \quad (4)$$

where $\mu, \nu = x, y$, D_t and D_r are, respectively, the translational and the rotational diffusion constants.

The torque τ in Eq. (2) is a key ingredient for the observation of stable orbits. For example, in models of circle swimmers, one typically consider a constant torque, induced by some built-in asymmetry of the swimmer's activation mechanism. When such particles are confined to, e.g., a harmonic trap, the interplay of persistent motion, confinement, and torque does give rise to a stable orbit in the weak noise

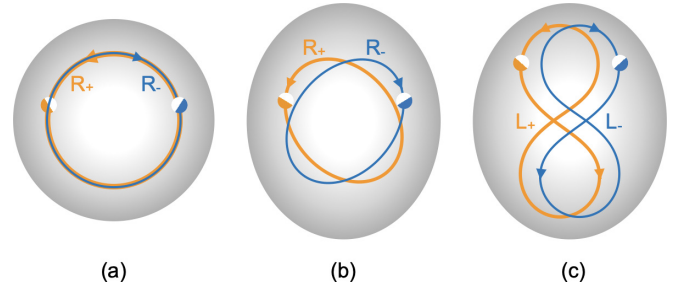


FIG. 1. Schematic zero-noise orbits of an active particle (half-filled dots) modeled by Eqs. (1), (2), and (5) for radially symmetric (a) and elliptic (b, c) confinement. The blank-to-filled direction in the dots indicates the propulsion direction, which is typically nontangential to the orbit. For the elliptic case, orbits of different shapes, such as ovals (a) and lemniscates (b) can coexist. The labels indicate orbits where the propulsion axis $\hat{\mathbf{n}}$ undergoes rotation (R) or libration (L) (see text). The $+/-$ subscripts indicate the sense of the orbit at the upper lobe as indicated by the arrows.

limit [32]. However, the shape and direction of the orbit of the circle swimmer are predetermined by τ . Therefore, there are no competing orbits in this case.

In contrast, for systems with aligning torque, the direction of the orbit is not decided a priori, but rather the symmetry is broken spontaneously as discussed below. This torque typically appears when the swimmer interacts with: confining walls, as in the cases of geometrically confined, motile bacteria and algae [28,29]; phoretic gradients, as in the case of self-propelled Janus particles [33]; or the potential induced by the combination of gravity and a curved surface, as in the case of the hexbug crawler on a parabolic antenna [30]. Typically, the aligning torque is modeled as [29,34]

$$\tau = b(\hat{\mathbf{n}} \times \mathbf{F}) \cdot \hat{\mathbf{z}}, \quad (5)$$

where b is a constant with dimension of length and \mathbf{F} is the local confining force. Notice that $\tau = 0$ when the particle climbs up the confining potential in a way that $\hat{\mathbf{n}}$ and \mathbf{F} are parallel to each other. However, for sufficiently high angular mobility β , this situation becomes unstable and the symmetry is spontaneously broken, as now the nonzero angle between $\hat{\mathbf{n}}$ and \mathbf{F} can be either positive or negative, resulting in a torque that can make the particle follow either clockwise (R_+) or counterclockwise (R_-) orbit [29,30], as illustrated in Fig. 1(a). In other words, the dynamics is now bistable. Furthermore, if the confining potential lacks rotation symmetry, there typically appears multiple metastable orbits with different topological properties coexisting in the same region of the space of parameters [31]. For example, an elliptic harmonic potential allows for the coexistence of ovals, where $\hat{\mathbf{n}}$ performs a full rotation (R), leading to a topological index $\oint_{\text{R}} d\theta = \pm 2\pi$, and lemniscates, where $\hat{\mathbf{n}}$ undergoes libration (L), that is, it swings back and forth without completing a full rotation, thus leading to $\oint_{\text{L}} d\theta = 0$. Notice that, for the elliptic potential, the equations of motion are invariant with respect to reflections in the x and y axes. Therefore, each orbit is accompanied by a twin which is its exact mirror image, giving a total of four coexisting orbits, as illustrated in Figs. 1(b) and 1(c).

B. Least-action principle and the most probable escape path

Each metastable orbit discussed above is associated with a basin of attraction, which is a region in phase space containing all the initial conditions that will lead to the orbit in the absence of noise. The boundary of the basin of attraction defines the separatrix that separates it from neighboring basins. During a noise-induced escape, the noise provides energy to the particle to abandon its current orbit and escape the corresponding basin of attraction through some point at the separatrix, where the escape process ends. This process can be viewed as a stochastic trajectory, the *escape path*, that connects the starting point of the escape to the point where the particle reaches the separatrix. When this process is finished, the particle enters a new basin of attraction and relaxes towards the new orbit.

The probability density of a particular escape path Γ can be estimated as follows [35]. Let dt be the time interval elapsed as the particle advances from point A at Γ to another point B infinitesimally close. The probability that B also lies at Γ is equal to the probability that the values of the Langevin forces are exactly those necessary for that end, that is, $P \propto \exp[-\frac{1}{4D}(\frac{1}{u}\xi^2 + \xi^2)dt]$, where, from here on, we parameterized the noise intensities as $D_r = D$ and $D_t = uD$. Therefore, the probability density of the specific escape path Γ is

$$\rho(\Gamma) = Ae^{-S(\Gamma)/D}, \quad (6)$$

where

$$S(\Gamma) = \frac{1}{4} \int_{\Gamma} \left(\frac{1}{u} \xi^2 + \xi^2 \right) dt \quad (7)$$

can be interpreted as the *action integral* and A is a normalizing factor. As $D \rightarrow 0$, the stochastic escape process is dominated by the most probable escape path (MPEP), that is, by the path Γ that minimizes the action integral and, thereby, maximizes the probability. The MPEP can be obtained in two steps: (i) finding the path $\Gamma_{o \rightarrow s}$ between two given endpoints, one at the orbit (o) and the other one at the separatrix (s), that minimizes $S_{o \rightarrow s}$; (ii) finding which one of the possible pairs of endpoints minimizes the action integral globally.

The minimization of S between two given endpoints can be performed by solving the corresponding Euler-Lagrange equations subjected to the constraints given by Eqs. (1) and (2). Here we choose the alternative Hamiltonian approach, which consists in substituting the probability density function in the form of Eq. (6) into the Fokker-Planck equation corresponding to the Langevin Eqs. (1) and (2):

$$\frac{\partial \rho}{\partial t} = uD \nabla^2 \rho + D \frac{\partial^2 \rho}{\partial \theta^2} - \nabla \cdot [\rho(v_0 \hat{\mathbf{n}} + \mu \mathbf{F})] - \beta \frac{\partial(\rho \tau)}{\partial \theta}. \quad (8)$$

In the low-noise ($D \rightarrow 0$) limit, we can expand Eq. (8) in powers of D and obtain, to lowest order, a partial differential equation for S ,

$$\begin{aligned} -\frac{\partial S}{\partial t} &= H\left(\mathbf{r}, \theta, \mathbf{p} = \nabla S, p_\theta = \frac{\partial S}{\partial \theta}\right) \\ &= (v_0 \hat{\mathbf{n}} + \mu \mathbf{F}) \cdot \mathbf{p} + \beta \tau p_\theta + u\mathbf{p}^2 + p_\theta^2. \end{aligned} \quad (9)$$

Equation (9) is formally equivalent to the Hamilton-Jacobi equation of a system described by the coordinates \mathbf{r} and θ

and their conjugate momenta \mathbf{p} and p_θ . Here, H represents the (Wentzel-Freidlin) Hamiltonian and S the classical action [36]. The corresponding Hamilton equations of motion are

$$\dot{\mathbf{r}} = v_0 \hat{\mathbf{n}} + \mu \mathbf{F} + 2u\mathbf{p}, \quad (10)$$

$$\dot{\theta} = \beta \tau + 2p_\theta, \quad (11)$$

$$\dot{\mathbf{p}} = -\mu \nabla(\mathbf{F} \cdot \mathbf{p}) - \beta(\nabla \tau)p_\theta, \quad (12)$$

$$\dot{p}_\theta = -v_0(\hat{\mathbf{z}} \times \hat{\mathbf{n}}) \cdot \mathbf{p} - \beta \frac{\partial \tau}{\partial \theta} p_\theta. \quad (13)$$

Therefore, given a starting point in the attraction basin arbitrarily close to the orbit, the escape trajectory is given deterministically by the solution of Eqs. (10)–(13). From Eq. (9), the stationarity of S requires that $H = 0$ (eikonal condition), that is, the escape path from a given initial condition is also a zero energy solution.

By comparing Eqs. (10) and (11) with Eqs. (1) and (2), one identifies the generalized momenta as $\mathbf{p} = \boldsymbol{\xi}/2u$ and $p_\theta = \xi/2$. This establishes the formal correspondence between the solutions obtained for \mathbf{p} and p_θ and the exact sequence of fluctuations necessary to assist the particle through the optimum path. Furthermore, the corresponding action can be obtained by integrating the Lagrangian $L = \mathbf{p} \cdot \dot{\mathbf{r}} + p_\theta \dot{\theta} - H$. Using Eqs. (10), (11), and (9), the Lagrangian can be reduced to $L = u\mathbf{p}^2 + p_\theta^2$, which leads to the same form of the action integral given by Eq. (7). Therefore, the MPEP is the path corresponding to the minimum action integral,

$$S = \min [S(\Gamma)] = \min \left[\int_{\Gamma} (u\mathbf{p}^2 + p_\theta^2) dt \right]. \quad (14)$$

III. TRANSITIONS BETWEEN METASTABLE CIRCULAR ORBITS

For radially symmetric confinement, $V(r)$, it is convenient to express the deterministic version of Eqs. (1) and (2) in terms of the polar coordinates, r and ϕ , and the tilt angle $\chi = \angle(\hat{\mathbf{n}}, \mathbf{r}) = \theta - \phi$. This way, r and χ form an independent subspace, described by the equations [31]

$$\dot{r} = v_0 \cos \chi - \mu V'(r), \quad (15)$$

$$\dot{\chi} = \left(\beta b F - \frac{v_0}{r} \right) \sin \chi, \quad (16)$$

while ϕ can be obtained straightforwardly from $\phi = v_0 \int dt r^{-1} \sin \chi$. These equations admit as steady state solutions two circular orbits of radius R , tilt angle $\chi = \pm \chi_0$, and constant angular speed $\dot{\phi} = \pm \omega$, where

$$R = \frac{v_0}{b\beta F(R)}, \quad (17)$$

$$\chi_0 = \arccos(\alpha), \quad (18)$$

$$\omega = \frac{v_0}{R} \sqrt{1 - \alpha}, \quad (19)$$

and $\alpha \equiv \mu/(bR\beta)$. The orbits are stable for any attractive confining potential, that is $V'(r) \geq 0, \forall r$, as long as $\alpha < 1$ [31]. Notice that in the limit $\alpha \rightarrow 1^-$ one has $\chi_0 = 0, \omega = 0$, and $V'(R) = v_0/\mu$, so that R coincides with the stall point and

the period of the orbit diverges. This corresponds precisely to the climbing phase. Therefore, by decreasing α from $\alpha > 1$, the climbing state ($\chi = 0$) gives place continuously to one of two equally stable orbiting states ($\chi = \pm\chi_0$), similar to spontaneous symmetry-breaking phase transitions observed in thermodynamic systems like an uniaxial ferromagnet.

A. Transitions in the hard-wall potential

Here we consider an active particle of radius R_p geometrically confined by a circular wall of radius R_w , similar to the experiments of Refs. [28] and [29]. In this kind of confinement, the particle interacts with the wall mainly via steric forces, so that $V'(r)$ is essentially zero for $r < R \simeq R_w - R_p$ and very large for $r > R$. This results in a large $V''(r)$ in the close vicinity of the orbit radius, which makes this problem essentially 1D, as shown below.

For small deviations ($\delta r, \delta\chi$) from the circular orbit and for $V''(R) \gg v_0/\mu R$, Eqs. (15) and (16) can be expressed as the following linear system:

$$\begin{bmatrix} \delta\dot{r} \\ \delta\dot{\chi} \end{bmatrix} \simeq \begin{bmatrix} -\mu V''(R) & -\omega R \\ \frac{\omega}{\alpha v_0} \mu V''(R) & 0 \end{bmatrix} \begin{bmatrix} \delta r \\ \delta\chi \end{bmatrix}. \quad (20)$$

The eigenvalues, $\lambda_1 = -\mu V''(R)$, associated with a mixed change of r and χ , and $\lambda_2 = -v_0\alpha(1 - \alpha^2)/R$, associated with displacements of χ without changing the orbit radius, are both negative, thereby guaranteeing the stability of the orbit. Furthermore, since $|\lambda_1| \gg |\lambda_2|$, changing the orbit radius is much harder than changing the tilt angle. Therefore, $\delta\dot{r} \simeq 0$, so that $\mu V' = v_0 \cos \chi$ at all times, and the dynamics can be described by a single approximate equation,

$$\dot{\chi} = f(\chi) + \xi = \frac{v_0}{\alpha R} \sin \chi (\cos \chi - \alpha) + \xi, \quad (21)$$

where now the deterministic term $f(\chi)$ depends only on χ and we add the orientational Langevin force ξ (the effect of translational fluctuations will be discussed later on).

Within the simplifications discussed above, the switching of the orbit direction can be seen as the noise-induced escape of a particle confined in a one-dimensional effective potential $\psi(\chi) = -\int f(\chi)d\chi$ or

$$\psi(\chi) = \frac{v_0}{2\alpha R} \cos \chi (\cos \chi - 2\alpha). \quad (22)$$

As shown in Fig. 2, the behavior of $\psi(\chi)$ nicely illustrates the spontaneous symmetry breaking taking place when $\beta > \mu/bR$ and giving rise to two degenerate local minima located at $\pm\chi_0$. The minimum at negative (positive) χ corresponds to the clockwise (counterclockwise) orbit. The decay of an orbit into the other occurs by noise-induced activation over the barrier located at $\chi = 0$. Therefore, the escape rate can be determined using Kramers formula for the effective potential $\psi(\chi)$. However, it is instructive to find the escape rate using the theory presented in Sec. II to check for its consistency.

For this 1d problem, the auxiliary Hamiltonian is $H = fp_\chi + p_\chi^2$ and the corresponding Hamilton equations are

$$\dot{\chi} = f(\chi) + 2p_\chi, \quad (23)$$

$$\dot{p}_\chi = -f'(\chi)p_\chi. \quad (24)$$

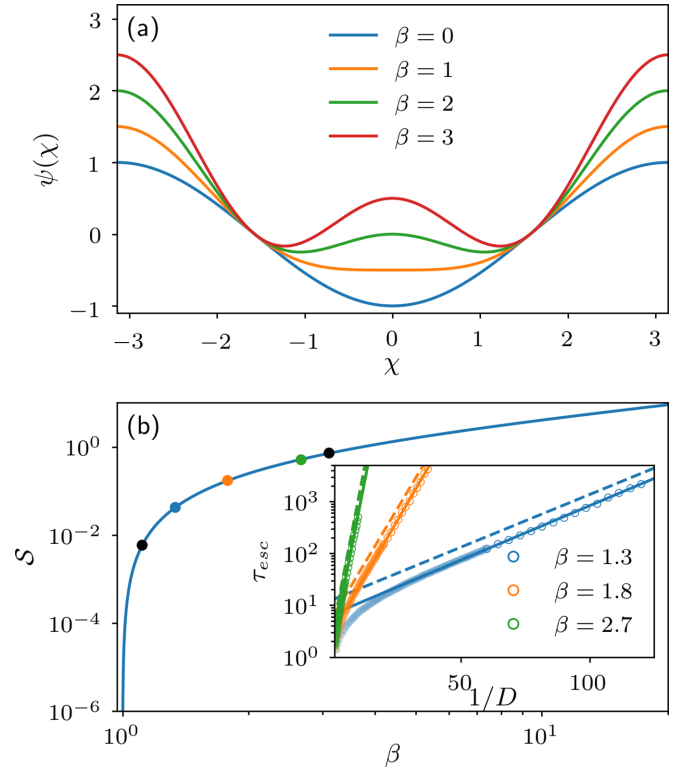


FIG. 2. (a) Effective potential ψ for an active particle in hard-wall confinement as a function of tilt angle χ for different values of the angular mobility β [Eq. (22), with $\alpha = \mu/(bR\beta)$]. (b) Minimum action for the switching between clockwise and counterclockwise orbits as a function of β [Eq. (26)]. Symbols are numerical estimates of activation energies obtained from direct simulations of the Langevin equations. Both S and ψ are in units of v_0/R and β is in units of μ/bR . Inset: semilog plot of the mean escape time, $\tau_{esc} = 1/k$, as a function of $1/D$ calculated from simulations (symbols) and analytically using Eq. (27) (dashes) for selected values of β . Open symbols correspond to the linear part of the data used for extracting the activation energy by an Arrhenius fitting (solid lines).

As discussed in the previous section, the MPEP must satisfy the eikonal condition, $H = 0$, which leads to a simple nontrivial solution for the conjugate momentum, $p_\chi = -f$. Substituting this result in Eq. (23), we obtain

$$p_\chi = \dot{\chi} = -f(\chi), \quad (25)$$

that is, the MPEP corresponds to the time-reversed version of the deterministic motion, as expected for a 1d escape problem. From Eqs. (14) and (25), the action integral along this path can be expressed as the difference in effective potential between the local minimum ($\chi = \pm\chi_0$) and the saddle point ($\chi = 0$),

$$S = -\int_{\chi_0}^0 f(\chi)d\chi = \psi(0) - \psi(\chi_0) = \frac{v_0(1 - \alpha)^2}{2\alpha R}. \quad (26)$$

This demonstrates the consistency of the MPEP approach, applied to the problem of an active particle in hard-wall circular confinement, with the classic Kramers theory for a Brownian particle in a 1d potential. In this case, the prefactor of the escape rate can be calculated using Kramers formula [37],

leading to

$$k = \frac{v_0 \sqrt{(1-\alpha)(1-\alpha^2)}}{2\pi\alpha R} \exp\left[-\frac{v_0(1-\alpha)^2}{2\alpha R D}\right]. \quad (27)$$

To validate these theoretical results, we performed numerical simulations of Eqs. (1) and (2) for a circular particle of radius R_p confined geometrically by a circular wall of radius R_w for different values of noise intensity D . The particle-wall interaction is modeled by a truncated Lennard-Jones (WCA) potential, $U(d) = 0$, for $d > 2^{1/6}$, and $U(d) = 4\epsilon(d^{-12} - d^{-6}) - \epsilon$, for $d < 2^{1/6}$, where $d = (R_w - r)/R_p$ is the reduced radial distance between the particle center and the wall. For each value of D , the equations of motion were integrated following a stochastic second-order Runge-Kutta algorithm starting from a perfect counterclockwise circular orbit all the way until the particle first crosses the separatrix, which in this case corresponds to the surface $\chi = 0$. The mean escape time, $\tau_{\text{esc}} = k^{-1}$, was then estimated by averaging the crossing time over 10^4 realizations of the stochastic force. Once D falls below a certain threshold, the $\tau_{\text{esc}}(1/D)$ data approaches the Kramers law, as illustrated in the inset of Fig. 2. The slope of the fit to the data points in the linear regime (unfilled points) is taken as an estimate of the activation energy. Finally, in Fig. 2(b), we show the agreement between the activation energy estimated from simulations and the analytical result Eq. (26).

B. Transitions in the harmonic potential and effect of translational noise

Here we consider a much softer kind of confinement, the parabolic well $V(r) = \frac{1}{2}\kappa r^2$. For this problem, circular orbits are the only stable attractors of the dynamics for $\beta > \beta_c \equiv \mu^2\kappa/bv_0$ and their radius and tilt angle are given by

$$R = R_{\text{stall}} \sqrt{\frac{\beta_c}{\beta}} \quad \text{and} \quad \chi_0 = \arccos \sqrt{\frac{\beta_c}{\beta}}, \quad (28)$$

where $R_{\text{stall}} = v_0/\kappa\mu$ is the stall point of the particle in the harmonic potential. In contrast to the hard-wall case, here the escape problem cannot be reduced to one dimension, requiring one to consider the full set of Eqs. (1) and (2) to correctly model the problem. Moreover, the right hand side of these equations cannot be expressed as the gradient of a potential, so Kramers rate formula does not work here. Therefore, it is necessary to find the MPEP by minimizing the action integral. We perform this task by solving Eqs. (10)–(13) starting from 10^5 random initial conditions in the close vicinity of the source orbit all the way up to the separatrix, which, by symmetry, corresponds to the $\phi = \theta$ ($\chi = 0$) plane in the $r\phi\theta$ phase space. For the initial conditions we fixed a point at the orbit, $(r, \phi, \theta) = (R, 0, \chi_0)$, and chose 10^5 different values of the momenta uniformly distributed on the surface of a sphere of radius 10^{-6} and centered at $(p_r, p_\phi, p_\theta) = (0, 0, 0)$. This shooting method allows for sampling different take-off directions, each one generating an escape path that minimizes the action locally. The MPEP is chosen as the one path that minimizes S globally.

In Fig. 3 we show the MPEP obtained by this method for different values of β (1.2, 1.6, and 2.0, in units of

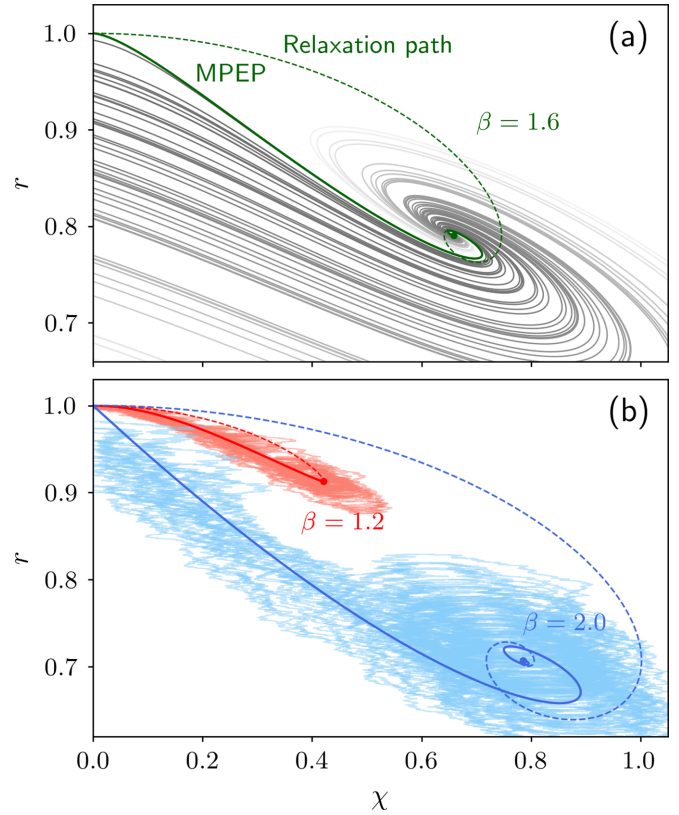


FIG. 3. The most probable escape path (solid line) from counterclockwise orbit and the relaxation path (dashes) towards clockwise orbit for an active particle in parabolic confinement for (a) $\beta = 1.6$ and (b) $\beta = 1.2$ and 2.0 . Grayscale lines in panel (a) are 50 randomly chosen nonoptimum escape attempts, which minimize the action S only locally; the lighter the line, the larger the action along the corresponding path. The transparent noisy lines in panel (b) depict a small subset of 20 escape trajectories obtained by numerically integrating the original stochastic problem for $\beta = 1.2$ (red) and 2.0 (blue). Here, r and β are expressed in units of $v_0/\kappa\mu$ and $\mu^2\kappa/bv_0$, respectively.

$\beta_c = \mu^2\kappa/bv_0$) and $u = 0$ (negligible translational noise). Notice that, since this problem is symmetric with respect to the variable ϕ , the escape problem can be fully described in the $r\chi$ plane, with the orbit being represented by a single point located at (R, χ_0) . A few remarkable points are readily noted: (i) for larger values of β , the MPEP presents a spiral shape, meaning that the escape trajectory typically wobbles around the circular orbit before reaching the boundary; (ii) the MPEP ends at the stall point, $(r, \chi) = (R_{\text{stall}}, 0)$, which thereby can be viewed as the saddle point for the escape; (iii) the relaxation from the saddle to the new orbit or back to the original one (dashed line) is not anti-parallel to the optimum escape path, which is a consequence of the time irreversibility of the system. In contrast, nonoptimal escape attempts [shown as gray-shaded lines in Fig. 3(a)] end up at a radial position $r < R_{\text{stall}}$. These paths have higher action integral (lighter shade of gray) and therefore are less probable routes.

To validate the MPEP approach applied to this particular example, we performed simulations of the Langevin equa-

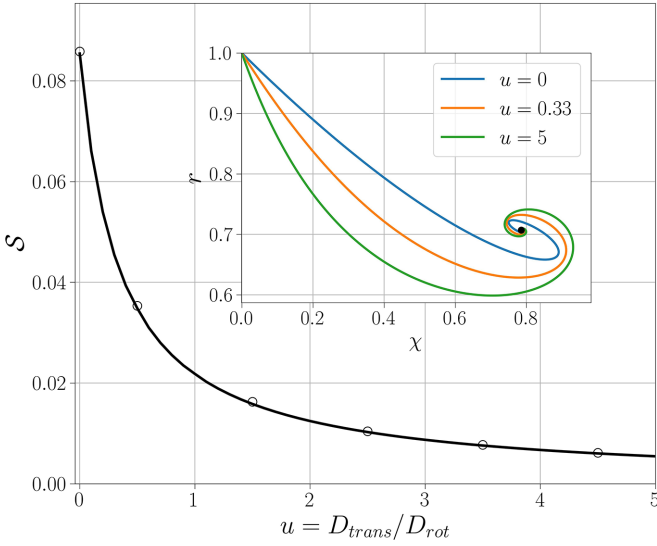


FIG. 4. Minimum action (in units of $1/\kappa\mu$) for the switching between clockwise and counterclockwise orbits of an harmonically trapped active particle as a function $u = D_t/D_r$ (in units of R_{stall}^2). Symbols correspond to activation energies estimated by fitting the low-noise data of direct Langevin simulations. Inset: MPEPs in the $r\chi$ plane calculated for a few selected values of u .

tions of motion and calculated the mean escape time τ_{esc} (averaged over 10^4 realizations) as a function of noise intensity D . As in the previous example, we estimated the low-noise activation energy of the escape by fitting the linear part of the $\log \tau_{\text{esc}}$ versus $(1/D)$ data. Once again, the numerically estimated activation energies are in excellent agreement with the action integral along the MPEP, as discussed in more detail further below. In Fig. 3(b), we compare the MPEP with 20 randomly chosen realizations of escape trajectories obtained by integrating the Langevin equations for $\beta = 1.2\beta_c$ ($D = 0.001$) and $\beta = 2.0\beta_c$ ($D = 0.01$). These values of D were chosen within the range where the $\log \tau_{\text{esc}}$ simulation data scales linearly with $1/D$. Although the escape trajectories are considerably noisy, they follow in average the theoretical MPEP and the escape through the boundary of the attraction basin takes place at points close to the stall point, as predicted by the minimum action principle.

C. Effect of translational noise

In thermal equilibrium, the translational and rotational noises acting on a spherical active particle are related by $u = D_t/D_r = \sigma^2/3$. Since in most cases of interest the particle diameter σ is small compared to other relevant length scales, the contribution of translational noise is often neglected, specially considering that other nonthermal noise sources usually contribute to decrease u even further [38]. For the case of confined active particles, the particle size is typically considerably smaller than the trapping region ($\sigma < R_{\text{stall}}$). Therefore, one typically has $u \ll R_{\text{stall}}^2$. Nevertheless, in what follows, we shall also consider $u > R_{\text{stall}}^2$ to have a broader picture of the effect of translational noise.

In Fig. 4, we present the action integrated along the MPEP as a function of u for fixed $\beta = 2\beta_c$. We also estimated

the activation energy from numerical simulation data of the Langevin equations for different values of u . As shown in Fig. 4, the simulation data points are in excellent agreement with the action integrated along the MPEP (line) in the full range of u values investigated. The results evidence a strong dependence of the MPEP and the corresponding minimum action on u . Overall, as u increases, the MPEP oscillates more violently around the circular orbit before reaching the boundary (inset), while the corresponding action integral decreases. In particular, for $u = 0.33R_{\text{stall}}^2$, which corresponds to a particle of radius $R_{\text{stall}}/2$ in thermal equilibrium, the action is approximately half the value observed for the $u = 0$ case.

IV. TRANSITIONS BETWEEN METASTABLE NONCIRCULAR ORBITS

Here, we turn our attention to transitions between noncircular orbits of an active particle trapped in the elliptic potential $V(x, y) = \frac{1}{2}\kappa(\frac{1}{1-e^2}x^2 + y^2)$, where e is the eccentricity. As shown in Ref. [31], this potential allows for the coexistence of a variety of orbits, of different shapes and topological indexes. To be specific, we focus on the case $e = 0.731$ and $\beta = 2.5\mu^2\kappa/bv_0$, where two reflection-symmetric oval orbits (R_+ and R_-) and two reflection-symmetric lemniscates (L_+ and L_-) coexist with each other, as shown in Fig. 5. Further, we assume negligible translational noise ($u = 0$).

The task of finding the MPEP in this case is considerably more challenging than in the previous examples. First, the basins of attraction are highly nontrivial, making it necessary to map them numerically. For that, we solved the noiseless version of Eqs. (1) and (2) for $\sim 2 \times 10^8$ initial conditions defined in a regular grid in the region $-1.5 < x < 1.5$, $-1.5 < y < 1.5$, $-\pi < \theta < \pi$ of phase space and classified each grid point according to which orbit the trajectory ends up. Second, the lack of rotational symmetry of the orbits makes it necessary to sample escape attempts taking off from different places of the orbit to find the MPEP. Accordingly, we integrated the Hamilton's Eqs. (10)–(13) from 10^7 takeoff points chosen randomly in the close neighborhood of the whole extension of the source orbit. For that, we chose 100 different points at the source orbit and for each of them we chose 10^5 different values of the momenta uniformly distributed on the surface of a sphere of radius 10^{-6} and centered at $(p_x, p_y, p_\theta) = (0, 0, 0)$. An example of MPEP calculated following this procedure is shown in Fig. 5 for the case where R_+ is the source orbit. The color background indicates projections of the attraction basins.

In principle, a full comprehension of the noise-induced transitions between these orbits requires investigating all 12 possible transitions. This complexity can be mitigated by considering the symmetry properties of the noiseless version of Eqs. (1) and (2). For the elliptic potential, these equations are invariant under π rotations, $(x, y, \theta) \rightarrow (-x, -y, \theta + \pi)$, and reflections in the x axis, $(x, y, \theta) \rightarrow (x, -y, -\theta)$. Therefore, to each escape path, there are three other paths that can be mapped exactly to the first one by some combination of these symmetry operations. For example, under a π rotation R_+ transforms to itself whereas L_- transforms to L_+ , as can be inferred from Fig. 5(a). Therefore, there exists a path from R_+ to L_+ that is identical to the MPEP from R_+ to L_- shown

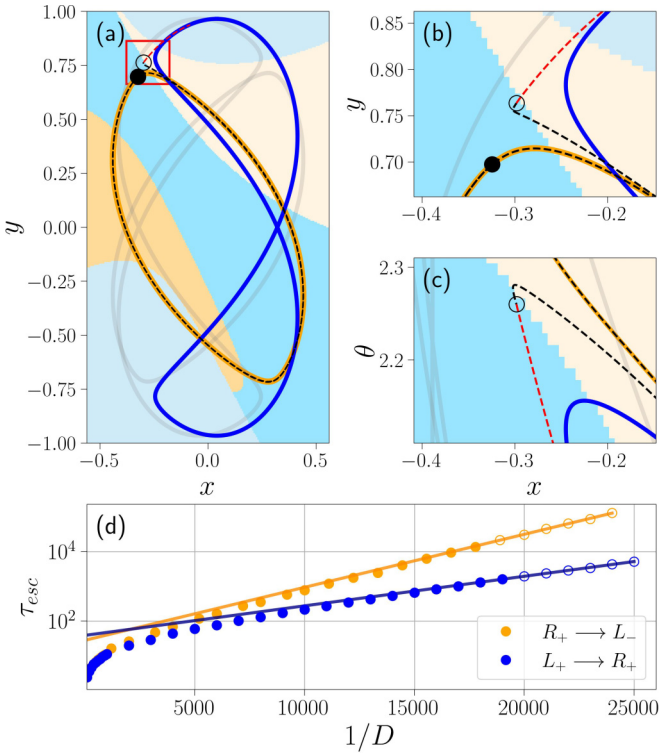
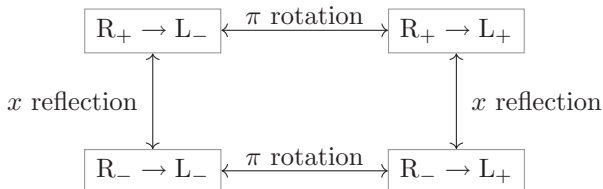


FIG. 5. (a) Most probable escape path (black dashes) from orbit R_+ (orange) and subsequent relaxation path (red dashes) towards L_- (blue). Also shown are orbits R_- and L_+ (gray transparent lines), which are not involved in this particular escape. The yellow, orange, blue and light blue backgrounds depict the attraction basins of R_+ , R_- , L_- , and L_+ respectively. The basins are projected on the xy plane at $\theta = 2.26$ rad, corresponding to the propulsion direction at the point where the escape trajectory first enters the attraction basin of the target orbit in all three projections, xy (b), $x\theta$ (c), and $y\theta$ (not shown). (d) Mean escape time τ_{esc} versus $1/D$ obtained from direct Langevin simulations of $R_+ \rightarrow L_{\pm}$ and $L_- \rightarrow R_{\pm}$ escapes (symbols). The open symbols were selected for Arrhenius fits (lines), which allowed us to estimate the activation energies $E_{R_+ \rightarrow L_-}^a = 3.5 \times 10^{-4}$ and $E_{L_- \rightarrow R_+}^a = 2.0 \times 10^{-4}$, remarkably close to the corresponding least actions, $\mathcal{S}_{R_+ \rightarrow L_-} = 3.4 \times 10^{-4}$ and $\mathcal{S}_{L_- \rightarrow R_+} = 1.9 \times 10^{-4}$.

in Fig. 5, but rotated by π . Similarly, other paths can also be found by performing symmetry operations as illustrated in the diagram below.



A crucial question is whether all the paths generated by these symmetry operations also minimize the action, that is, are all of them MPEPs? To be MPEP, each of them must be an equivalent solution of the least-action problem. Notice that the Hamilton's equations are not invariant under the rotation and reflection operations defined above. However, we can extend them to the six-dimensional Hamiltonian phase space by also requiring that $(p_x, p_y, p_\theta) \rightarrow (-p_x, -p_y, p_\theta)$ under π rotations

and $(p_x, p_y, p_\theta) \rightarrow (p_x, -p_y, -p_\theta)$ under x reflections. This way, Hamilton's equations (10)–(13) are fully invariant and so is the action integral, since it is insensitive to the sign of the conjugate momenta. Therefore, all four transitions are degenerate MPEPs, that is, they produce the same least-action integral. This was indeed verified within the numerical accuracy of our least-action calculations, where we found $\mathcal{S}_{R_+ \rightarrow L_-} = 3.4 \times 10^{-4} (\kappa\mu)^{-1}$. Analogously, all four escapes from libration to rotation can also be recovered from a single one, say L_- to R_+ . In this case, our MPEP calculation leads to $\mathcal{S}_{L_- \rightarrow R_+} = 1.9 \times 10^{-4} (\kappa\mu)^{-1}$, revealing that, in general, escapes from R to L are not symmetrical to escapes from L to R .

These observations were confirmed by direct simulations of the Langevin equations, which resulted in similar number of escapes from R_+ to L_- and from R_+ to L_+ in the full range of investigated noise values as well as approximately the same value of activation energy estimated from the low noise data [see Fig. 5(d)]. The same applies for escapes from L orbits. The activation energies for both $L \rightarrow R$ and $R \rightarrow L$ escapes were estimated from Arrhenius fitting the $\log \tau_{esc}$ versus $1/D$ data, averaged over 5×10^3 independent realizations of the problem. As in the previous examples, the activation energies are in good agreement with the action integral over the corresponding MPEPs.

Finally, we also calculated optimum escape paths between orbits of the same species. These escapes are obviously symmetrical, in the sense that $R_+ \rightarrow R_-$ has the same action integral as $R_- \rightarrow R_+$. However, for the chosen values of β and e , direct transitions between orbits of same species have considerably higher action integral: $\mathcal{S}_{R_+ \rightarrow R_-} \simeq 350\mathcal{S}_{R_+ \rightarrow L_-}$ and $\mathcal{S}_{L_- \rightarrow L_+} \simeq 10\mathcal{S}_{L_- \rightarrow R_+}$. Therefore, at the low noise limit, a full reversal of the R_+ (L_+) orbit towards its twin R_- (L_-) is only possible by first visiting the attraction basin of one of the lemniscate (oval) orbits, that is $R_+ \rightarrow L_{\pm} \rightarrow R_-$ ($L_+ \rightarrow R_{\pm} \rightarrow L_-$). Indeed, in our simulations of the Langevin equations, escapes between orbits of the same species are never observed for $D < 10^{-3}$. Of course, these results are not general, as the hierarchy of the most probable target orbits might change completely for other values of the system parameters β and e .

V. CONCLUSIONS

In this study, we introduced a method rooted in the least-action principle to rigorously investigate the noise-induced escape of active particles from metastable orbits in the low-noise limit. We methodically analyzed transitions between various dynamical orbits spanning different confinement scenarios. From transitions between basic clockwise and counterclockwise circular orbits in radially symmetric traps to more complex orbits in elliptic confinements, our theoretical results align consistently with direct numerical simulations based on the Langevin equations of motion.

The formalism we presented not only simplifies the task of accurately determining the activation energy tied to orbital transitions but also offers pivotal insights. One salient revelation is that under low-noise conditions, particles adhere to a well-defined trajectory: the most probable escape path. This path is intricately influenced by various system parameters, such as angular and translational mobilities, self-propulsion

velocity, and the specific nature of the confining potential. Furthermore, the derived Hamiltonian equations possess symmetry properties essential for pinpointing degenerate escape paths and for establishing a hierarchy amidst multiple competing orbits.

Our findings open avenues for expanded research on the dynamical properties of confined active matter. Potential directions include exploring noise-induced escapes from chaotic orbits and investigating synchronization phenomena. Beyond these theoretical prospects, our results hold potential significance for practical applications. Active particles, due to their persistent motion, can get ensnared in specific dynamical states. Such patterns, while intriguing, can introduce complications in real-world scenarios, like drug delivery, where

specific behaviors or trajectories are desired. Unveiling the role of noise on switching between different dynamical states can shed light on new strategies for manipulating particle behaviors for specific tasks.

ACKNOWLEDGMENTS

We thank L. R. E. Cabral for useful discussions. This work was financed in part by Coordenação de Aperfeiçoamento de Pessoal de Nível Superior-Brasil (CAPES), Finance Code 001. C.C.S.S. is funded by Conselho Nacional de Desenvolvimento Científico e Tecnológico-Brasil (CNPq), Grant No. 312240/2021-0.

-
- [1] H. A. Kramers, Brownian motion in a field of force and the diffusion model of chemical reactions, *Physica* **7**, 284 (1940).
 - [2] L. I. McCann, M. Dykman, and B. Golding, Thermally activated transitions in a bistable three-dimensional optical trap, *Nature (London)* **402**, 785 (1999).
 - [3] R. L. Kautz, Activation energy for thermally induced escape from a basin of attraction, *Phys. Lett. A* **125**, 315 (1987).
 - [4] J. A. Blackburn, H. J. T. Smith, and N. Grønbech-Jensen, Chaos and thermal noise in a Josephson junction coupled to a resonant tank, *Phys. Rev. B* **53**, 14546 (1996).
 - [5] L. J. Lapidus, D. Enzer, and G. Gabrielse, Stochastic phase switching of a parametrically driven electron in a penning trap, *Phys. Rev. Lett.* **83**, 899 (1999).
 - [6] K. Kim, M.-S. Heo, K.-H. Lee, H.-J. Ha, K. Jang, H.-R. Noh, and W. Jhe, Noise-induced transition of atoms between dynamic phase-space attractors in a parametrically excited atomic trap, *Phys. Rev. A* **72**, 053402 (2005).
 - [7] A. Longtin, A. Bulsara, and F. Moss, Time-interval sequences in bistable systems and the noise-induced transmission of information by sensory neurons, *Phys. Rev. Lett.* **67**, 656 (1991).
 - [8] I. A. Khovanov, A. V. Polovinkin, D. G. Luchinsky, and P. V. E. McClintock, Noise-induced escape in an excitable system, *Phys. Rev. E* **87**, 032116 (2013).
 - [9] P. S. Burada and B. Lindner, Escape rate of an active Brownian particle over a potential barrier, *Phys. Rev. E* **85**, 032102 (2012).
 - [10] A. Geiseler, P. Hänggi, and G. Schmid, Kramers escape of a self-propelled particle, *Eur. Phys. J. B* **89**, 175 (2016).
 - [11] A. Sharma, R. Wittmann, and J. M. Brader, Escape rate of active particles in the effective equilibrium approach, *Phys. Rev. E* **95**, 012115 (2017).
 - [12] L. Caprini, U. Marini Bettolo Marconi, A. Puglisi, and A. Vulpiani, Active escape dynamics: The effect of persistence on barrier crossing, *J. Chem. Phys.* **150**, 024902 (2019).
 - [13] E. Woillez, Y. Zhao, Y. Kafri, V. Lecomte, and J. Tailleur, Activated escape of a self-propelled particle from a metastable state, *Phys. Rev. Lett.* **122**, 258001 (2019).
 - [14] K. S. Olsen, L. Angheluta, and E. G. Flekkøy, Escape problem for active particles confined to a disk, *Phys. Rev. Res.* **2**, 043314 (2020).
 - [15] D. Wexler, N. Gov, K. O. Rasmussen, and G. Bel, Dynamics and escape of active particles in a harmonic trap, *Phys. Rev. Res.* **2**, 013003 (2020).
 - [16] A. Militaru, M. Innerbichler, M. Frimmer, F. Tebbenjohanns, L. Novotny, and C. Dellago, Escape dynamics of active particles in multistable potentials, *Nat. Commun.* **12**, 2446 (2021).
 - [17] Y. Li, F. Marchesoni, T. Debnath, and P. K. Ghosh, Two-dimensional dynamics of a trapped active Brownian particle in a shear flow, *Phys. Rev. E* **96**, 062138 (2017).
 - [18] T. Debnath, Y. Li, P. K. Ghosh, and F. Marchesoni, Active microswimmers in a finite two-dimensional trap: The role of hydrodynamic interaction, *J. Chem. Phys.* **150**, 104102 (2019).
 - [19] B. ten Hagen, S. van Teeffelen, and H. Löwen, Brownian motion of a self-propelled particle, *J. Phys.: Condens. Matter* **23**, 194119 (2011).
 - [20] M. C. Marchetti, J. F. Joanny, S. Ramaswamy, T. B. Liverpool, J. Prost, M. Rao, and R. A. Simha, Hydrodynamics of soft active matter, *Rev. Mod. Phys.* **85**, 1143 (2013).
 - [21] C. Bechinger, R. Di Leonardo, H. Löwen, C. Reichhardt, G. Volpe, and G. Volpe, Active particles in complex and crowded environments, *Rev. Mod. Phys.* **88**, 045006 (2016).
 - [22] A. Pototsky and H. Stark, Active Brownian particles in two-dimensional traps, *Europhys. Lett.* **98**, 50004 (2012).
 - [23] Y. Fily, A. Baskaran, and M. F. Hagan, Dynamics of self-propelled particles under strong confinement, *Soft Matter* **10**, 5609 (2014).
 - [24] S. C. Takatori, R. De Dier, J. Vermant, and J. F. Brady, Acoustic trapping of active matter, *Nat. Commun.* **7**, 10694 (2016).
 - [25] K. Malakar, A. Das, A. Kundu, K. V. Kumar, and A. Dhar, Steady state of an active Brownian particle in a two-dimensional harmonic trap, *Phys. Rev. E* **101**, 022610 (2020).
 - [26] M. Caraglio and T. Franosch, Analytic solution of an active Brownian particle in a harmonic well, *Phys. Rev. Lett.* **129**, 158001 (2022).
 - [27] U. Nakul and M. Gopalakrishnan, Stationary states of an active Brownian particle in a harmonic trap, *Phys. Rev. E* **108**, 024121 (2023).
 - [28] T. Ostapenko, F. J. Schwarzendahl, T. J. Bøddeker, C. T. Kreis, J. Cammann, M. G. Mazza, and O. Bäümchen, Curvature-guided motility of microalgae in geometric confinement, *Phys. Rev. Lett.* **120**, 068002 (2018).
 - [29] A. Codutti, M. A. Charsooghi, E. Cerdá-Doñate, H. M. Täieb, T. Robinson, D. Faivre, and S. Klumpp, Interplay of surface interaction and magnetic torque in single-cell motion of magnetotactic bacteria in microfluidic confinement, *Elife* **11**, e71527 (2022).

- [30] O. Dauchot and V. Démery, Dynamics of a self-propelled particle in a harmonic trap, *Phys. Rev. Lett.* **122**, 068002 (2019).
- [31] R. H. Damascena, L. R. E. Cabral, and Clecio C. de Souza Silva, Coexisting orbits and chaotic dynamics of a confined self-propelled particle, *Phys. Rev. E* **105**, 064608 (2022).
- [32] S. Jahanshahi, H. Löwen, and B. ten Hagen, Brownian motion of a circle swimmer in a harmonic trap, *Phys. Rev. E* **95**, 022606 (2017).
- [33] B. Liebchen and H. Löwen, Which interactions dominate in active colloids? *J. Chem. Phys.* **150**, 061102 (2019).
- [34] I. S. Aranson and A. Pikovsky, Confinement and collective escape of active particles, *Phys. Rev. Lett.* **128**, 108001 (2022).
- [35] R. Feynman, A. Hibbs, and D. Styer, *Quantum Mechanics and Path Integrals*, Dover Books on Physics (Dover Publications, Mineola, NY, 2010).
- [36] M. Freidlin, J. Szucs, and A. Wentzell, *Random Perturbations of Dynamical Systems*, Grundlehren der mathematischen Wissenschaften (Springer, New York, NY, 2012).
- [37] H. Risken and H. Haken, *The Fokker-Planck Equation: Methods of Solution and Applications Second Edition* (Springer, Berlin, 1989).
- [38] J. Elgeti, R. G. Winkler, and G. Gompper, Physics of microswimmers-single particle motion and collective behavior: A review, *Rep. Prog. Phys.* **78**, 056601 (2015).